



Sea ice drift variability in Arctic Ocean Model Intercomparison Project models and observations

Torge Martin¹ and Rüdiger Gerdes¹

Received 30 March 2006; revised 18 October 2006; accepted 6 November 2006; published 23 March 2007.

[1] Drift is a prominent parameter characterizing the Arctic sea ice cover that has a deep impact on the climate system. Hence it is a key issue to both the remote sensing as well as the modeling community, to provide reliable sea ice drift fields. This study focuses on the comparison of sea ice drift results from different sea ice-ocean coupled models and the validation with observational data in the period 1979–2001. The models all take part in the Arctic Ocean Model Intercomparison Project (AOMIP) and the observations are mainly based on satellite imagery. According to speed distributions, one class of models has a mode at drift speeds around 3 cm s^{-1} and a short tail toward higher speeds. Another class shows a more even frequency distribution with large probability of drift speeds of 10 to 20 cm s^{-1} . Observations clearly agree better with the first class of model results. Reasons for these differences are manifold and lie in discrepancies of wind stress forcing as well as sea ice model characteristics and sea ice-ocean coupling. Moreover, we investigated the drift patterns of anticyclonic and cyclonic wind-driven regimes. The models are capable of producing realistic drift pattern variability. The winter of 1994/1995 stands out because of its maximum in Fram Strait ice export. Although export estimates of some models agree with observations, the corresponding inner Arctic drift pattern is not reproduced. The reason for this is found in the wind-forcing as well as in differences in ocean velocities.

Citation: Martin, T., and R. Gerdes (2007), Sea ice drift variability in Arctic Ocean Model Intercomparison Project models and observations, *J. Geophys. Res.*, *112*, C04S10, doi:10.1029/2006JC003617.

1. Introduction

[2] The spatial redistribution of sea ice is an important process in the climate system. The formation of leads and polynyas is mostly due to the movement of sea ice. Since the area of open water has a strong influence on the heat exchange between ocean and atmosphere, sea ice drift has an important effect on the local temperature of atmosphere and ocean. The same is true for the position of the sea ice edge that depends on the supply of sea ice from the interior ice pack. During the growth of sea ice salt is released to the ocean and freshwater instead during melting of the ice. Sea ice drift means a transport of freshwater and latent heat that importantly effects the oceanic salt and heat balance on a supra-regional scale. Moreover shear and convergent sea ice motion lead to deformation of the ice cover and therefore have an essential impact on the sea ice thickness.

[3] Sea ice drift is thus an important parameter that should be faithfully reproduced in sea ice-ocean models and coupled climate models. Besides ice concentration, which permits the derivation of ice area and extent, sea ice drift is the only variable that has been routinely

measured from satellites since the late 1970s. Ice concentration in AOMIP models is discussed by *Johnson et al.* [2007]. Measurements of sea ice drift have much improved through better methods to derive drift speed from moving structures between successive satellite images and through the introduction of microwave imagery [*Emery et al.*, 1997; *Maslanik et al.*, 1998]. Sea ice drift has been used extensively for the validation of sea ice rheologies in the Sea Ice Model Intercomparison Project (SIMIP) [*Lemke et al.*, 1997; *Kreyscher et al.*, 2000].

[4] Here we compare sea ice drift from two satellite products [*Fowler*, 2003; *Ezraty and Piollé*, 2004] and buoy data [*Ortmeyer and Rigor*, 2004] with a number of AOMIP model results for the period of satellite coverage. The observations are presented in the next section. There we also attempt to review the reliability of the data and their applicability for the comparison and validation of the sea ice model components in the AOMIP models. The models that enter the comparison are briefly introduced in the following section. Results in section 4 are based on histograms that provide the probability distribution of sea ice drift speed over the periods 1979–2001 and 1992–2001. We also provide histograms of deviations in drift speed and direction and composite sea ice drift patterns for different meteorological regimes. A discussion regarding the representation of sea ice drift in current models, the origin and the climatic significance of different model results is given in section 5.

¹Alfred Wegener Institute for Polar and Marine Research, Bremerhaven, Germany.

We conclude with recommendations for sea ice model parameters and validation data.

2. Observational Sea Ice Drift Data

[5] As sea ice drift observations, we use two satellite products that cover the periods 1979–2001 and 1992–2001, respectively. Data for the longer period are provided by the National Snow and Ice Data Center (NSIDC). Namely, we use the monthly mean gridded fields of the Polar Pathfinder Project [Fowler, 2003]. These sea ice drift vector fields are a composite of daily drift computed from Advanced Very High Resolution Radiometer (AVHRR), Scanning Multichannel Microwave Radiometer (SMMR), Special Sensor Microwave/Imager (SSM/I) satellite images and buoys of the International Arctic Buoy Program (IABP). The product has a spatial resolution of 25 km and is projected on the Equal-Area Scalable Earth (EASE) grid, which covers the entire Arctic. A second satellite derived drift product is obtained from the Centre ERS d'Archivage et de Traitement (CERSAT). Here we choose a merged product of Quick Scatterometer (QuikSCAT) and SSM/I derived sea ice drift vector fields [Ezraty and Piollé, 2004], which are projected on a grid that is oriented exactly as NSIDC's SSM/I-12.5-km grid but with a spatial resolution of 62.5 km and covering the central Arctic only. The monthly means are a composite of the 3-day or 6-day products in this case. The NSIDC and CERSAT products differ in the way sea ice drift is treated before public release. The NSIDC offers a sea ice drift field constructed by including nonsatellite information and readily interpolated at all grid nodes. The NSIDC data are available for each day of the year. The CERSAT product, on the other hand, contains drift estimates only at those locations, where satellite information is available and the estimates have passed certain filter routines. Thus CERSAT provides data, which is closer to the raw measurements but contains more gaps compared to the NSIDC product. From both these data sets we include only those monthly averaged data points in our investigation that were compiled from at least 25 of 30 days (80% temporal data coverage). Owing to the selection of the sources for the drift derivation, the CERSAT data are only available during the winter season, October to April. Passive microwave radiometers are sensitive to the columnar atmospheric water content and sea ice/snow surface melting that restricts the retrieval of reliable drift estimates to the period from October to April [Kwok *et al.*, 1998; Maslanik *et al.*, 1998].

[6] The satellite derived sea ice drift data are not direct observations and are afflicted with considerable uncertainty. Therefore we additionally included monthly mean drift estimates that we derived from raw position data of single buoys of the IABP [Ortmeyer and Rigor, 2004]. Although the buoy data set has a rather poor spatial coverage, 20–30 buoys with a spacing of 300–600 km are available each year [Rigor *et al.*, 2002], it represents the most exact drift measurements that are accessible at the moment. The standard error of the buoy positions that are derived with the Argos satellite system is less than 300 m [Rigor *et al.*, 2002]. Buoy position data are provided since 1979 mainly in 12 h intervals. We were able to calculate between 50 (first half of the 1980s) and 300 (first half of the 1990s) monthly

drift estimates for each year. In the period 1979–2001 most estimates are from October (380) and least from January (240). The spatial coverage of the buoys is most dense in the central Arctic Ocean and in the Beaufort Sea but sparse in the Eurasian marginal seas.

[7] Different sea ice drift products from satellite observations show differences that are manifest in the modal ice speed and speed distribution, expressed in a histogram, as well as the drift pattern. The latter is shown in Figure 1 for the winter mean of 1994/95, which stands out for its large Fram Strait ice export [Vinje *et al.*, 1998]. The NSIDC and CERSAT data sets agree on a spatially confined Beaufort Gyre, a cyclonic drift field extending from the Laptev Sea, and a broad Transpolar Drift Stream. Mean drift vectors compiled from buoy positions at the beginning and end of that winter support this pattern. To investigate the speed distribution characteristics we apply histograms of monthly averaged speed at the end of the winter (March) and summer season (October). In March, when the Arctic sea ice cover is closed and small speeds prevail, the differences between the data sets are comparatively small (Figure 2a). The modal speeds of all three observational data sets agree within a narrow range of 0.5–1.5 cm s⁻¹. During October, after the melting season, the ice cover is less dense and the ice is able to move faster and more freely. This characteristic is more expressed in the CERSAT and buoy data. Owing to its selection criteria the CERSAT data does not cover the entire Arctic at each time step and mainly coastal data is rare. Thus small speeds are underrepresented, as can be seen in Figure 2b in comparison with the distribution of all NSIDC data of October. This “coastal factor” is conceivably also the reason for the better match of the buoy drift estimates and the CERSAT data, even though the NSIDC data set incorporates buoy data. Moreover, under loose ice conditions a buoy represents the drift of a single ice floe rather than a mean drift of an area of 10²–10³ km², which is the typical grid cell or pixel size of model and satellite products.

3. Model Results Entering the Comparison

[8] From the AOMIP coordinated analysis experiment [Holloway *et al.*, 2007] we had monthly mean sea ice drift results available from five groups (National Aeronautics and Space Administration (NASA) Goddard Space Flight Center (GSFC) in Greenbelt, Maryland, USA; Institute of Ocean Science (IOS) in Sydney, British Columbia, Canada; Alfred Wegener Institute (AWI) in Bremerhaven, Germany; Naval Postgraduate School (NPS) in Monterey, California, USA and University of Washington (UW) in Seattle, Washington, USA). The sea ice dynamics are all based on work by Hibler [1979] except for those of the NPS model. The latter uses the elastic-viscous-plastic (EVP) rheology of Hunke and Dukowicz [1997]. Although all other models apply the viscous-plastic rheology of the original Hibler model individual implementations differ in details. Parameters that affect sea ice dynamics like the strength of the ice also vary among the models (see Table 1), whereas the atmosphere-sea ice and sea ice-ocean drag coefficients, $(1.1 + 0.04 \cdot u_s) \cdot 10^{-3}$ (where surface wind velocity u_s is measured in m s⁻¹) and $5.5 \cdot 10^{-3}$ respectively, are prescribed. The atmospheric drag depends on the surface wind u_s and a

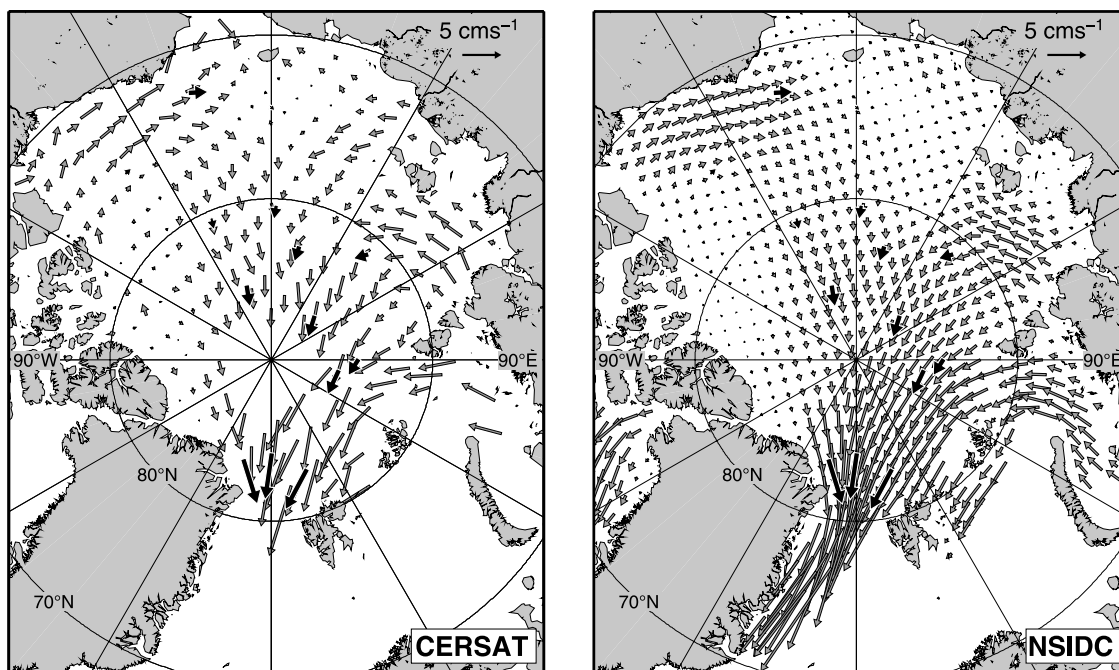


Figure 1. Maps of the Arctic sea ice drift field as represented in observational data from (left) CERSAT and (right) NSIDC. An average of winter 1994/1995 (November–April) is shown, and both data sets have been reduced for clarity. Additionally, bold black vectors mark the mean drift of buoys of the IABP that fully cover the same period.

quadratic drag law is prescribed for the ocean-ice drag. The models also differ in the individual ocean components (AWI and IOS use the Modular Ocean Model (MOM), GSFC uses the Princeton Ocean Model (POM), NPS and UW use the Parallel Ocean Program model (POP)) and the coupling of sea ice and ocean models. The atmospheric forcing is prescribed in detail within AOMIP although some groups deemed small deviations from the protocol necessary. The sea ice drift is strongly depending on the wind-forcing. Here the surface wind is calculated from the sea level pressure (SLP) data of the National Centers for Environmental

Prediction (NCEP) and National Center for Atmospheric Research (NCAR) reanalysis data [Kalnay *et al.*, 1996] as follows: first the geostrophic wind, with absolute velocity u_g , is derived and then this is retarded by a factor of 0.8 ($u_g < 15.0 \text{ m s}^{-1}$) or 0.7 (else) and turned by 30° ($u_g < 15.0 \text{ m s}^{-1}$) or 20° (else) to the left. In the GSFC and NPS model, however, an atmospheric drag coefficient of $1.1 \cdot 10^{-3}$ independent of the wind speed is applied and in the IOS model, wind stress values from the NCEP/NCAR reanalysis were used directly. The GSFC model further differs in the oceanic drag, where a description after Mellor and Kantha [1989] is

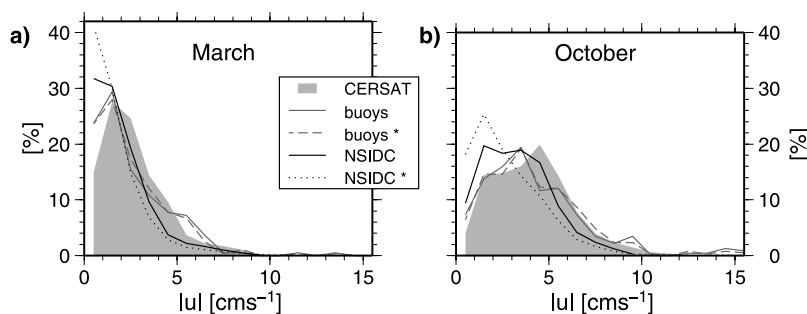


Figure 2. Histograms of observed sea ice drift speed for (a) March and (b) October of the interior Arctic. The CERSAT data of the period 1992–2001 are shown in gray shade. Additionally, drift speed distributions are presented for two NSIDC based data sets, one that corresponds to the CERSAT data locations and time period (NSIDC) and a second that includes all grid nodes within the interior Arctic and spans the full time period 1979–2001 (NSIDC*). Furthermore, equivalent data from the IABP buoys of the period 1992–2001 (buoy) and 1979–2001 (buoy*) are incorporated. Percentage values of the ordinate correspond to histogram bins along the abscissa with a bin width of 1 cm s^{-1} beginning at 0 cm s^{-1} . Lines of linear interpolation between bin values are shown instead of stairs-step diagrams for clarity reasons. The legend applies for Figures 2a and 2b.

Table 1. Participating Models and Some of Their Sea Ice Parameters^a

Model	Ice Strength P^* , $\cdot 10^4 \text{ N m}^{-2}$	Lead Closing Parameter h_0 , m	Ice Thickness Mean, m	Ice Thickness std, m
AWI	1.5	0.5	1.5	1.14
GSFC	1.0 ^b	0.25	1.2	1.72
IOS	2.0	0.3	2.1	1.50
NPS	2.75	0.5	1.7	1.14
UW	2.75	0.5	1.2	0.72

^aIce strength is a parameter of the *Hibler* [1979] model that enters the calculation of compression and shear strength of the ice. The lead closing parameter h_0 determines the demarcation between lateral and basal freezing. The mean and standard deviation (std) of ice thickness is calculated for the whole Arctic Ocean area including all marginal seas and Barents Sea for the period 1979–2001.

^bThis value holds for 3.3 m of ice thickness h ($P^* = 3 \cdot h \cdot 10^3$).

used instead. In an additional experiment the same AWI model is forced with different atmospheric forcing. In this experiment (hereafter: AWI 10-m-wind) the wind stress has been calculated from the wind at 10 m height provided by NCEP/NCAR reanalysis and not derived via the geostrophic wind.

4. Results

[9] To characterize the sea ice drift properties in the different models we rely on histograms of sea ice drift speed and maps of sea ice drift for certain situations. Sea ice drift maps will be shown for cyclonic and anticyclonic circulation regimes after *Proshutinsky and Johnson* [1997] as well as for the winter 1994/1995 that was characterized by very strong positive North Atlantic Oscillation (NAO) forcing and an extremely high sea ice export through Fram

Strait [*Vinje et al.*, 1998]. These two case studies represent well the typical experimental application and scaling of the AOMIP models. Because the sea ice volume budget of the Arctic is sensitive to the circulation regimes [*Martin and Martin*, 2006], the vorticity of the Beaufort Gyre is examined over the entire period of investigation as a measure of these regimes.

[10] The seasonal histograms for the period 1979–2001 are shown in Figure 3. Drift speeds below 0.5 cm s^{-1} have been discarded. This speed bin would otherwise dominate the speed distribution in some models. Almost all of the corresponding data stem from grid points that are very close to land or from semi-enclosed bays. Satellite data for those regions are usually not available or prone to large errors such that validation of those model results is not possible with current data. Furthermore, the geometry of the models differs for reasons that are independent of the sea ice dynamics (e.g., horizontal resolution and related choices of the modeling groups). Especially the Canadian archipelago is characterized by thick ice and very small drift speeds even in models with high resolution. Thus we decided to simplify the comparison by compiling the histograms only for speeds above 0.5 cm s^{-1} . Additionally, the drift speed estimates contributing to the histograms are selected from an area (sectors $70^\circ\text{N}–90^\circ\text{N}$, $50^\circ\text{E}–270^\circ\text{E}$ and $80^\circ\text{N}–90^\circ\text{N}$, $90^\circ\text{W}–50^\circ\text{E}$) excluding the marginal ice zone in the Greenland and Barents Sea as well as the entire sea ice cover of the Baffin Bay and Labrador Sea. This selected area represents the “interior Arctic”, which is of major interest to the regional climate model community. The marginal ice zone to the Nordic seas is excluded, because uncertainties of observational data and the variations in ice

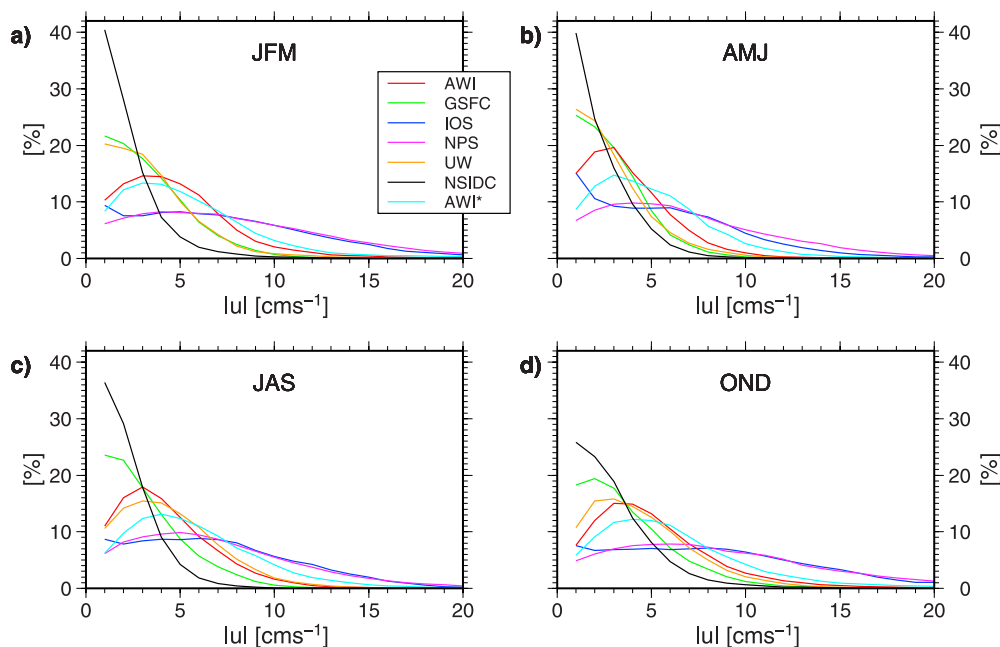


Figure 3. Seasonal histograms (a) January–March, (b) April–June, (c) July–September, and (d) October–December of sea ice drift speed for the interior Arctic for the period 1979–2001 for the AOMIP models. Corresponding distributions for the AWI 10-m-wind experiment (AWI*) and observations from NSIDC have been included. Bin width is 1 cm s^{-1} beginning at 0.5 cm s^{-1} , and the legend in Figure 3a applies also for Figures 3b–3d.

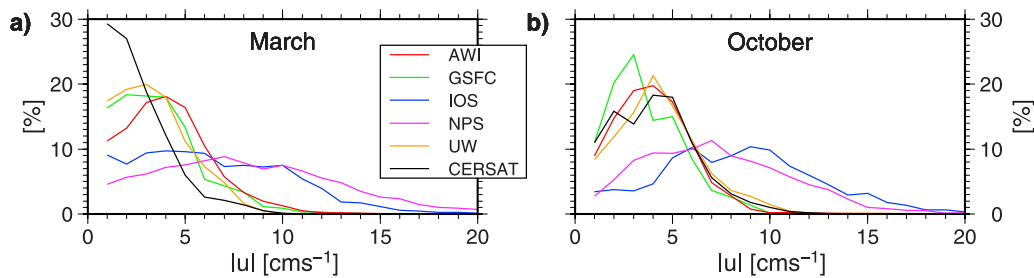


Figure 4. Histograms of sea ice drift speed of the interior Arctic for the AOMIP models and CERSAT observations for (a) March and (b) October of the period 1992–2001. Bin width is 1 cm s^{-1} beginning at 0.5 cm s^{-1} , and the legend applies for Figures 4a and 4b.

concentration and velocity between models is largest here. Ice extent in the models depend largely on the inflow of warm Atlantic water, simulated by the underlying ocean model, which is not subject of this study.

[11] Three models (AWI, GSFC, and UW) exhibit a mode at speeds below or equal to 3 cm s^{-1} and a relatively rapid decay toward high speeds (see Figure 3). In these models, sea ice speeds above 10 cm s^{-1} occur almost exclusively in summer and early fall. Two models (IOS and NPS) have a much lower frequency of occurrences of low speeds (below 5 cm s^{-1}) and a rather flat distribution with relatively large values at speeds between 10 and 20 cm s^{-1} . The AWI 10-m-wind experiment results in a speed distribution that shows a stage between both groups of AOMIP models. The histogram shows additionally the distribution of the NSIDC observations, which are best matched by the first group of models. The mode at or below 1 cm s^{-1} is only reproduced by the GSFC model and partly by the UW model (only during winter and spring).

[12] Similar results are obtained for the period 1992–2001 for which we have drift statistics based on the CERSAT observations. Since summer values are not available, we show in Figure 4 the monthly histograms for March and October as typical for seasonal extremes. Even in these months, the satellite data do not cover the whole domain. Model statistics have been derived for those grid nodes for which we have corresponding observations. From Figure 2 we already noted for the NSIDC data that the results in general are not significantly changed by this restriction, though small speeds are underrepresented in October. Especially, the differences between the two groups of models discussed above are a robust feature.

[13] In both months, the observations show virtually no sea ice speeds above 10 cm s^{-1} . In March, speeds between 1 and 2 cm s^{-1} have the highest observed frequency of occurrence. Model distributions are generally broader at low drift speeds and show more grid points with speeds at the fast end of the distribution. None of the models reproduces the large number of low speed points indicated by the observations. The IOS and NPS models have a considerable number of occurrences at speeds above 10 cm s^{-1} .

[14] For October, we find a shift of the observed maximum to higher speeds (see Figure 4b). There is a rapid drop in the frequency of occurrence at 6 cm s^{-1} . The AWI, GSFC, and UW models capture this behavior. Compared to these observations the IOS and NPS models again have too

many occurrences of very high speeds and too little grid points with speeds in the range below 5 cm s^{-1} .

[15] Velocity error histograms (Figure 5) corroborate the above results and exhibit the clearest impression on the splitting into two groups of model results. The AWI, GSFC, and UW models have symmetric distributions around zero error speed. On the other hand, the IOS and NPS models are biased toward high speeds. The differences in drift direction between models and CERSAT data are presented in Figure 5, too. Obviously the differences in speed do not bias the direction of the drift as the difference angle distributions do not separate into the two speed groups. Though all distributions have a clear mode at zero deviation, difference angles of up to 90° occur. Again, the AWI 10-m-wind results show larger differences from the observations than the AWI AOMIP run. Errors in this experiment are, however, still smaller than those in the IOS and NPS models. Especially the mode of the speed differences is still close to 0.0 cm s^{-1} (Figure 5f). Differences in speed and direction between the two satellite data sets (not shown) are markedly smaller than between model results and either product. Still, differences between the satellite products amount up to 60° in drift direction in a few cases. Larger differences in drift direction are restricted to smaller drift speeds. We define an “upper envelope” speed as the median speed over all grid points for which absolute angle differences larger than 45° occur. Upper envelope speeds differ between models (AWI: 2.4 cm s^{-1} , GSFC: 1.6 cm s^{-1} , IOS: 4.5 cm s^{-1} , NPS: 4.7 cm s^{-1} and UW: 2.0 cm s^{-1}) and give another handle to estimate the quality of the models. Normalizing these values by dividing them through the mean of the largest 10% of all speed estimates of a model data set, yields for nearly all models a ratio of around 0.3. Only the GSFC model shows a better performance with a ratio of 0.2.

[16] Maps of sea ice drift for different circulation regimes and the differences in drift between them are shown in Figure 6 for the AWI and NPS models. These models are taken as representatives of the two groups of AOMIP models identified above. The maps are composites for the anticyclonic and cyclonic circulation regimes (ACCR and CCR, respectively) of *Proshutinsky and Johnson* [1997] and *Proshutinsky et al.* [2002] during the winters between 1979 and 2001. These composites of the months November to April separate into the ACCR years 1979, 1984–1988 and 1998–2001 and the CCR years 1980–1983 and 1989–1997. Despite basic similarities between the regimes

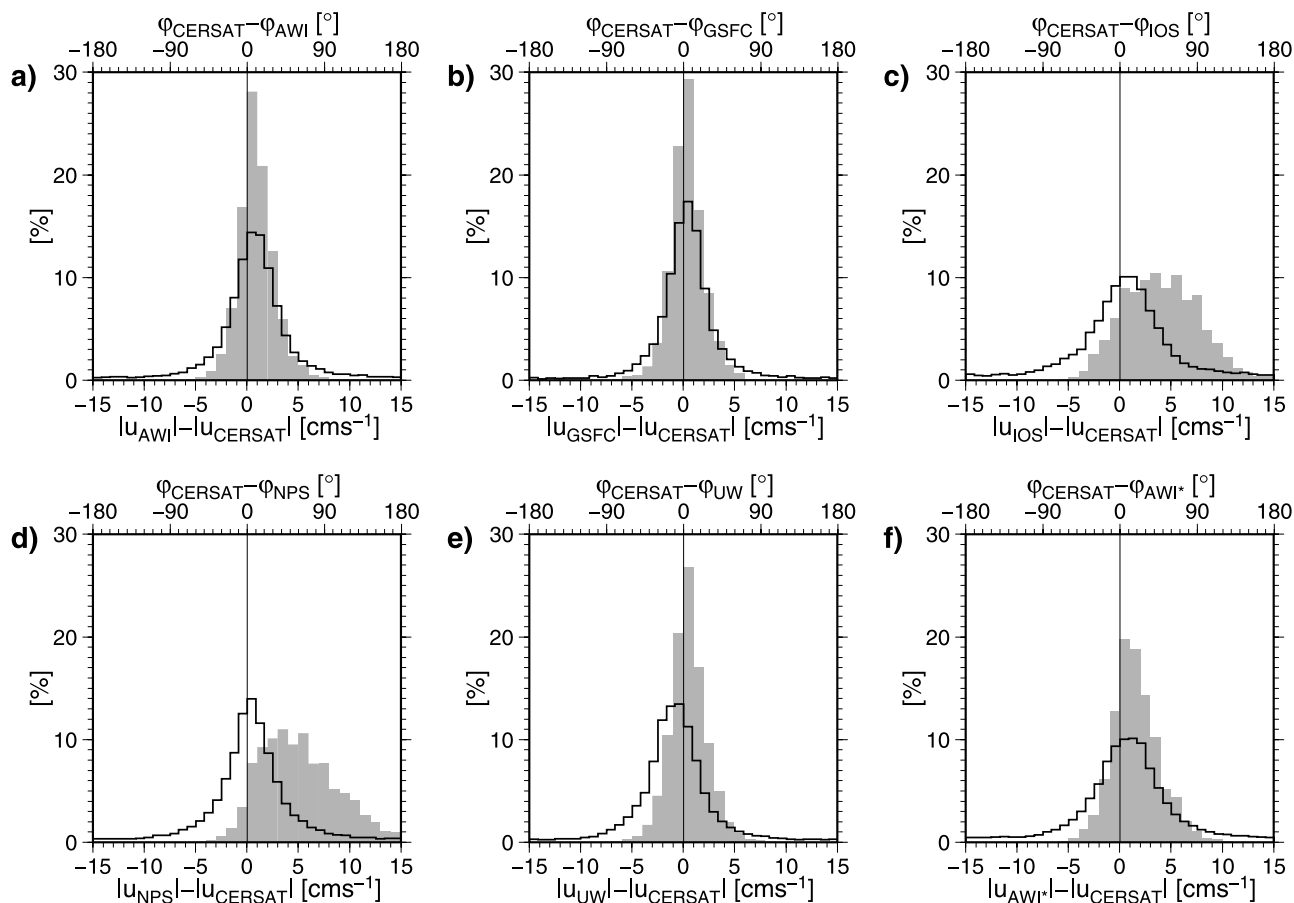


Figure 5. Histograms for the difference between model and satellite derived (CERSAT) sea ice drift speeds (gray shade) and direction (black outline). These histograms refer to the period 1992–2001. Only the months January–April and October–December are considered because of lack of satellite data for the summer months. The models are (a) AWI, (b) GSFC, (c) IOS, (d) NPS, and (e) UW. (f) Same differences for the AWI 10-m-wind experiment (here: AWI*). Differences in direction are presented as angle of deviation between the corresponding drift vectors: positive (negative) value means deviation of the model data to the right (left) of the satellite-derived vector.

(a persistent anticyclonic direction of rotation in the Beaufort Gyre and a southward flow in the Fram Strait and Greenland Sea), both models show pronounced differences between the circulation regimes. The NPS model shows a weaker Beaufort Gyre with its center shifted toward Alaska during the CCR. With this shift comes an eastward displacement of the transpolar drift. However, the Beaufort Gyre is still a well-pronounced, closed feature in this model result. The export pattern of sea ice from the Laptev Sea changes between regimes and is turned from a northwest to a northward direction. Sea ice is directed more straight to the Fram Strait in the ACCR. Drift speeds in the Barents, Kara and Laptev Seas increase during the CCR.

[17] The AWI model shows similar differences between circulation regimes to the NPS model. As seen above, sea ice speeds are generally smaller in the AWI model for both circulation regimes. This model exhibits almost a breakdown of the Beaufort Gyre during the CCR with a reversal of the sea ice motion in the western East Siberian Sea. The transpolar drift reaches farther into the Makarov and Canadian Basin than in the NPS model result during the CCR. The ice export direction out of Laptev Sea changes in the

AWI model in the same direction as in the NPS results, but from northward to a northeast direction. Associated with the pronounced shift of the transpolar drift is a change in the sea ice drift direction and speed between Greenland and the North Pole. In the CCR phase more thick multiyear ice from north of Greenland and Ellesmere Island, formed during the ACCR phase, is transported toward Fram Strait, indicating a strong sensitivity of the Fram Strait ice export to the atmospheric forcing over the Arctic Ocean. Furthermore, there is a pronounced southwestward ice export out of the Barents Sea during the CCR detectable in the AWI results.

[18] The differences in absolute drift speed between the two regimes are twice as large in the NPS results (-4 to $+4$ cm s^{-1}) than in the AWI data (-2.5 to $+2$ cm s^{-1}), which starts from smaller absolute speeds. Normalizing these differences by the modal speed averaged over both regimes, 2.5 cm s^{-1} for AWI and 6.0 cm s^{-1} for NPS, results in drift speed difference ratios of the range -0.8 to $+0.8$ equal in pattern for both models. The models' sea ice drift speed does not only differ in the long-term mean but also in the sensitivity to anomalous forcing. The response in the direction of the drift is very similar, on the other hand.

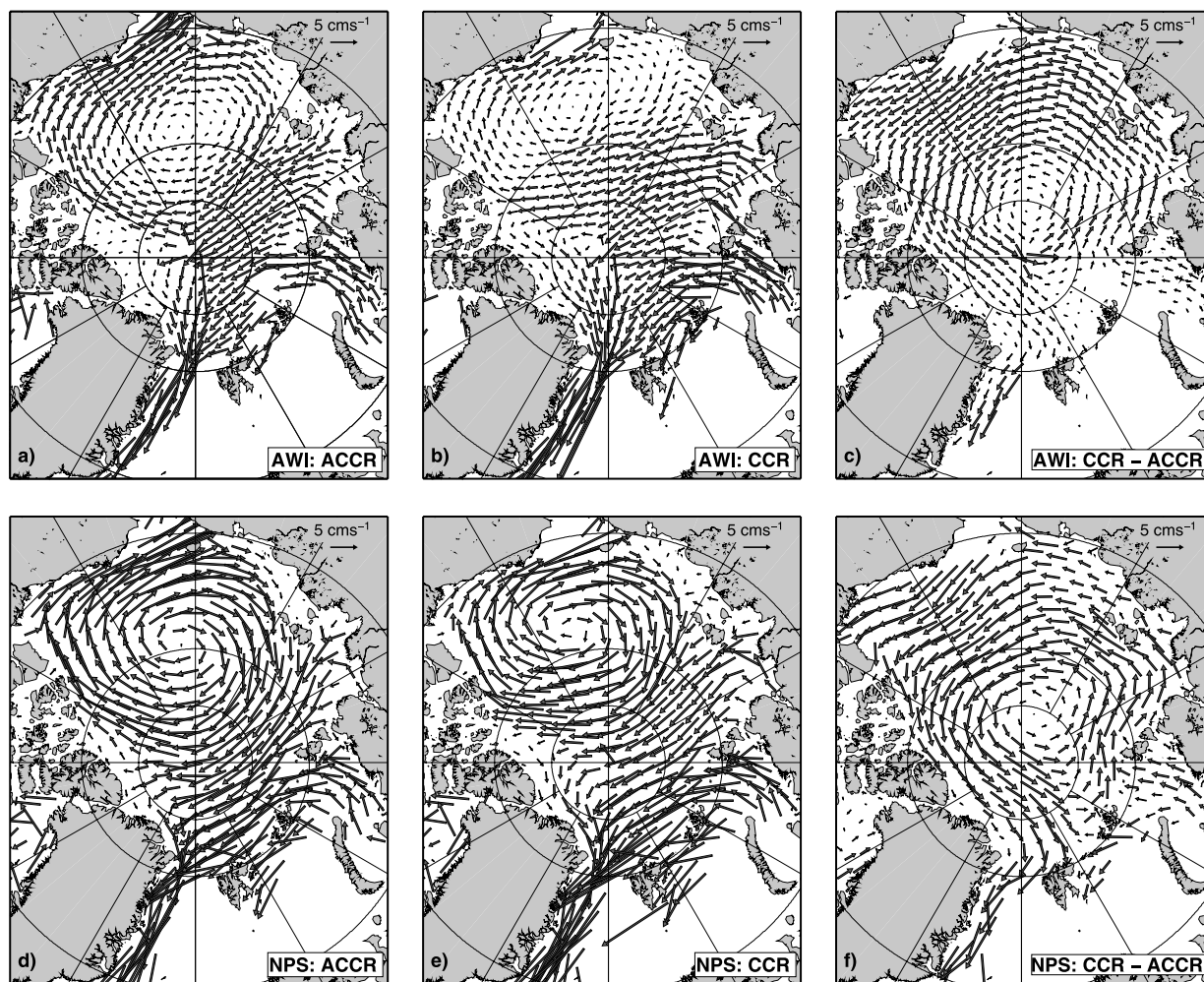


Figure 6. Composite maps of winter sea ice drift for the (left) anticyclonic circulation regime (ACCR) and the (middle) cyclonic circulation regime (CCR) [Proshutinsky and Johnson, 1997; Proshutinsky et al., 2002]. (right) Differences in drift velocity between the regime composites. (top) Results from the AWI model and (bottom) results from the NPS model. For clarity reasons the horizontal resolution is individually reduced and changing spatial coverage is due to particular ice extent.

[19] We calculated the vorticity of the sea ice motion in the Beaufort Gyre in order to show the variability of this dominant feature of the Arctic sea ice drift in the different data sets. Because the model data are given on different grids we chose four fixed positions to derive one value of vorticity for each month: for the u-component (74°N , 170°W) and (84°N , 170°W) and for the v-component: (78°N , 160°E) and (78°N , 140°W). The calculations result in a time series that is presented for the AWI and the NPS model, representing the two model groups, in Figure 7. Both models feature strong seasonal and interannual variability. The average of the so defined vorticity is negative because the anticyclonic Beaufort Gyre dominates the region. However, there are short phases, when cyclonic drift prevails, especially in the years 1994 and 1995. In order to integrate all model data sets and also the observations from NSIDC in the vorticity comparison, the mean values of each of the four regime phases falling into the period of our investigation are calculated for each data set (see Table 2). However, none of the models show a clear shift in mean vorticity between the two regimes but all

feature the extreme cyclonicity of the 1989–1997 phase. The average vorticities derived from the observations do not reflect the regimes as clearly as the model results.

[20] Finally, we present the period November 1994 to April 1995 as a single winter mean that stands out for its large Fram Strait ice export. The composite maps of observed sea ice drift for this winter were presented in Figure 1. All AOMIP models fail to reproduce the observed drift pattern of the winter 1994/95. Especially the results of AWI, GSFC and IOS differ considerably from the observed drift pattern in the sector 150°E – 330°E (see AWI results in Figure 8a as a representative result). These models show a close correlation between sea ice drift and the SLP field (see Figure 8d). Though belonging to different groups concerning the absolute drift speeds NPS and UW models feature a pattern that is closer to the observational data (see Figures 8b and 8c). This is evident, for example, in the Beaufort Sea. Here the impact of the low in the central Arctic is weaker and the dominant cyclonic gyre is weakened to an extent that an extremely retreated anticyclonic Beaufort Gyre is visible in the Beaufort Sea. The ice drift

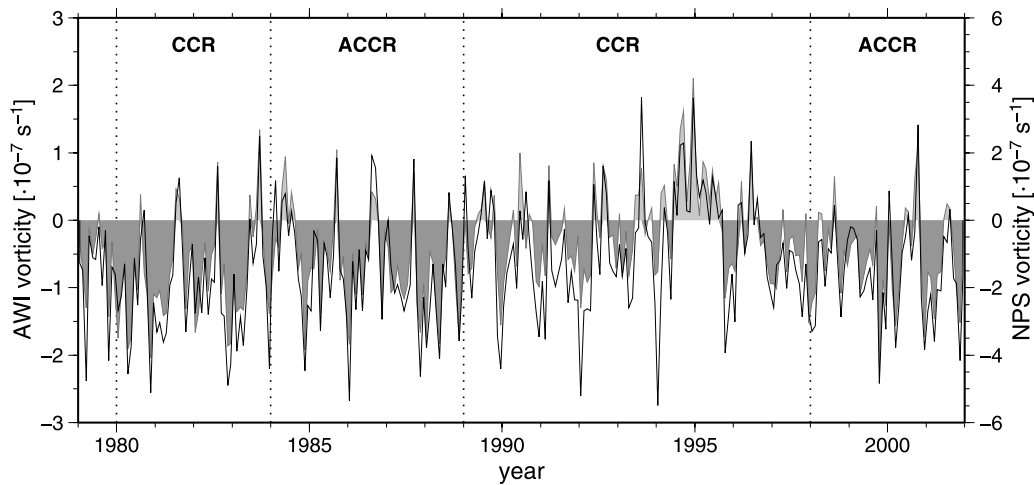


Figure 7. Time series of the vorticity of the Beaufort Gyre. Results from the AWI model are shown in gray shade (left axis scaling) and those of the NPS model are shown as black outline (right axis scaling). The regime phases of the wind-driven circulation after *Proshutinsky et al. [2002]* are separated by dotted lines and labeled at the top. Year annotations indicate January 1.

along the Alaskan coast is directed opposite to the other AOMIP results. This compares well to the observations. Nevertheless, modeled drift speed and direction deviate from the observations in the East Siberian Sea and central Arctic. The result of the AWI 10-m-wind run (Figure 8e) differs considerably from the one forced accordingly to AOMIP protocol and is generally closer to the observed drift, resembling the NPS result. Besides the changed pattern in the Beaufort Sea the AWO 10-m-wind experiment features also smaller drift speeds in the East Siberian and Laptev seas compared to the AWI AOMIP run. However, the changed wind-forcing does not dispose of the central cyclonic gyre. Here the embedded buoy drift vectors indicate, that the frontier between the remnants of the Beaufort Gyre and the dominant cyclonic gyre in the modeled drift fields is located too far to the east.

5. Discussion

[21] From the analysis of sea ice drift speed statistics we can distinguish two groups of model results, one that is relatively close to observations and one where sea ice speeds are overestimated. The two observational data sets correspond to each other much more than the models do. Differences between models from different groups are also clearly larger than the differences between the model results of the first group and observations. That modeled drift

speeds exceed observed is in good agreement with the results of *Martin and Martin [2006]*, who found a difference of 1.0 cm s^{-1} between modeled and satellite derived modal drift speeds on a monthly scale. Their uncoupled sea ice model is comparable to the one used in the AWI coupled version here. Also, *Thomas [1999]* supports a bias of 1.0 cm s^{-1} between standard model configurations, matching the AOMIP model specifications best, and daily buoy data. What is the cause of these striking differences between model results? The main contributions to the sea ice momentum balance are the wind-forcing, the ocean-ice drag, the internal stresses, and the Coriolis force [*Harder et al., 1998*]. In the region of the Beaufort Gyre the sea surface pressure gradient force may reach the same magnitude as the Coriolis force and can therefore not be neglected there. However, this local momentum balance cannot explain the overall differences in the drift speed distributions. Different settings of other parameters, like the ice strength parameter P^* and the lead closing parameter h_0 do not separate clearly into the two groups (see Table 1). However, the ice strength parameter P^* enters the equation for the ice strength P scaled by an exponential function of the ice concentration A of the form $\exp(C(1 - A))$, where C is a constant [*Hibler, 1979*]. This makes the ice strength sensitive to small variations of A for values above 90%. For the interior Arctic (as defined in section 4) we found that the NPS model features ice concentrations not larger than 98%

Table 2. Mean Vorticity Values of the Different Data Sets Separated for the Four Periods of Different Circulation Regimes Covered by This Study and Overall Correlation of the Time Series to the Observations of the NSIDC

Data Set	CCR (1980–1983) Vorticity, $\cdot 10^{-7} \text{ s}^{-1}$	ACCR (1984–1988) Vorticity, $\cdot 10^{-7} \text{ s}^{-1}$	CCR (1989–1997) Vorticity, $\cdot 10^{-7} \text{ s}^{-1}$	ACCR (1998–2001) Vorticity, $\cdot 10^{-7} \text{ s}^{-1}$	Correlation Coefficient to NSIDC
AWI	−0.80	−0.62	−0.14	−0.54	0.64
GSFC	−0.44	−0.39	−0.15	−0.53	0.68
IOS	−1.55	−0.86	−0.88	−1.29	0.53
NPS	−2.06	−1.48	−0.90	−1.55	0.68
UW	−0.84	−0.64	−0.49	−0.63	0.65
NSIDC	−0.44	−0.29	−0.31	−0.34	(1.0)

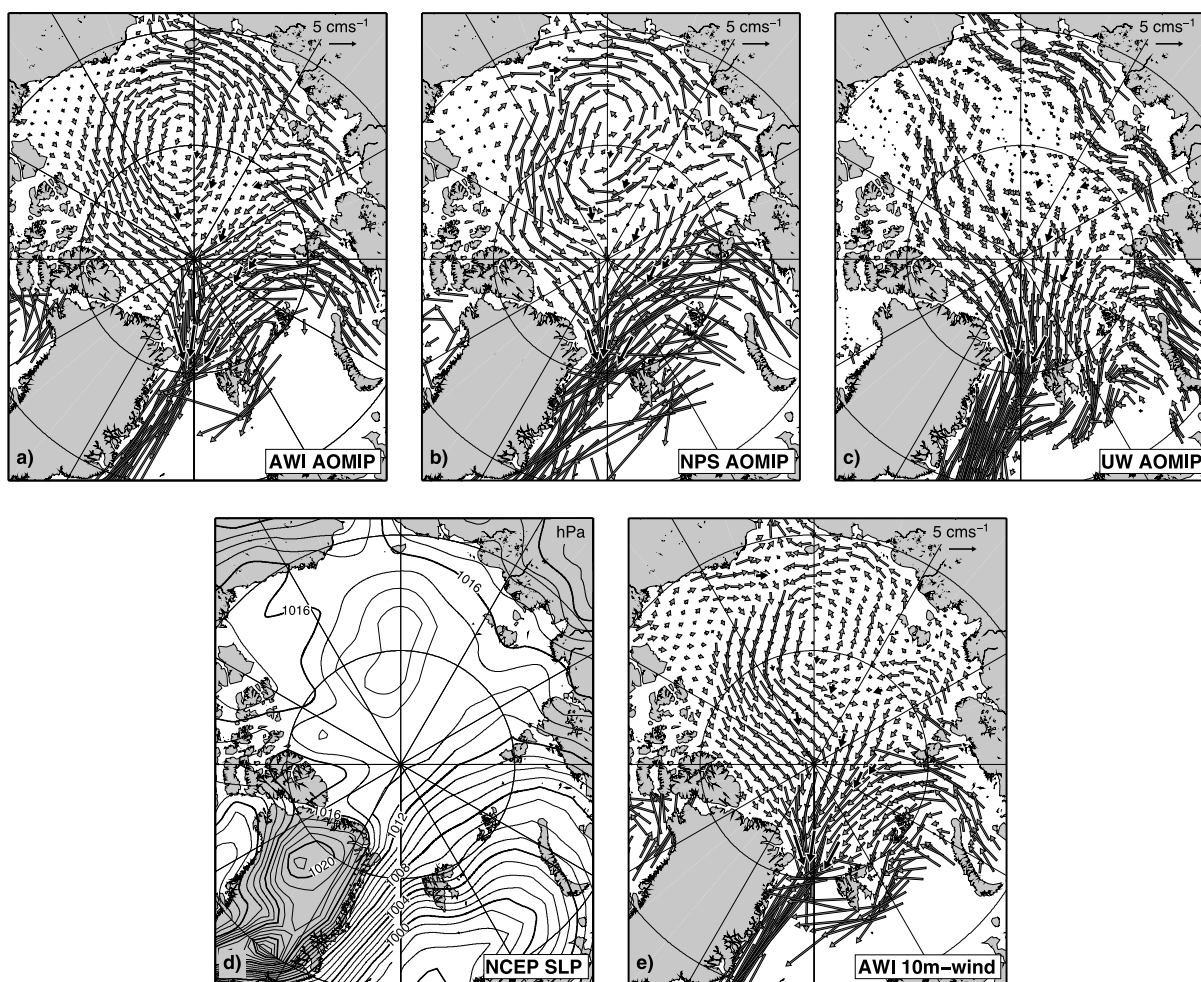


Figure 8. Sea ice drift velocity averaged over the winter (November–April) of 1994/1995 from AOMIP models (a) AWI, (b) NPS, and (c) UW and (d) the corresponding NCEP/NCAR reanalysis sea level pressure field. (e) Sea ice drift of this winter from the AWI 10-m-wind experiment. Figures 8a, 8b, 8c, and 8e include IABP buoy drift vectors in bold black. For clarity reasons the horizontal resolution of modeled data is individually reduced and changing spatial coverage is due to particular ice extent.

on average even in winter. The UW model's ice concentration exceeds 99%. Since both models have the same P^* , this difference in mean ice concentration definitely contributes to larger ice speeds in the NPS model. Contradictory are the findings regarding the ice thickness. High sea ice speeds occur preferentially for thin ice and low ice concentrations. Under these conditions, the internal stresses are negligible. We expect that a thinner ice cover would lead to faster ice drift. Models of group one, which agree well with the observations all exhibit moderate mean ice thicknesses of 1.2 to 1.5 m. On the other hand, both the IOS and the NPS model of the second group of models feature thicker ice. Sea ice thickness and rheology are apparently not responsible for the main model differences. In contrast, higher drift speeds due to the chosen forcing are able to increase sea ice thickness dynamical via deformation.

[22] Regarding the possible causes of the differences in sea ice drift between the two model groups we cannot exclude the atmospheric forcing variables completely though they are prescribed identically according to AOMIP specifications. Some exchange parameters are fixed by the

AOMIP protocol, namely the atmospheric and oceanic drag coefficients. However, there are important details of the implementation of atmospheric and oceanic forcing that differ between models, among them the actual prescription of the wind stress, differences in ocean currents, and the implementation of the ocean-ice drag term. From Figure 8 it has become clear that wind stresses derived from SLP and the corresponding reanalysis product lead to different sea ice drift results. In general the wind stress calculated after AOMIP prescriptions is found to be weakest, followed by a moderate increase in strength for the 10-m-wind derived stresses, which also show differences in direction. Yielding the same pattern the momentum flux from NCEP/NCAR reanalysis is again stronger than the 10-m-wind derived stresses. The winter 1994/1995 sea ice drift pattern turned out to be more realistic in the AWI model when 10-m-wind derived stresses were used instead of AOMIP wind stresses. However, the AWI model using AOMIP-derived stresses has a more realistic sea ice speed distribution than when driven with 10-m-wind derived stresses. We tentatively conclude that the differences in constructing wind stress

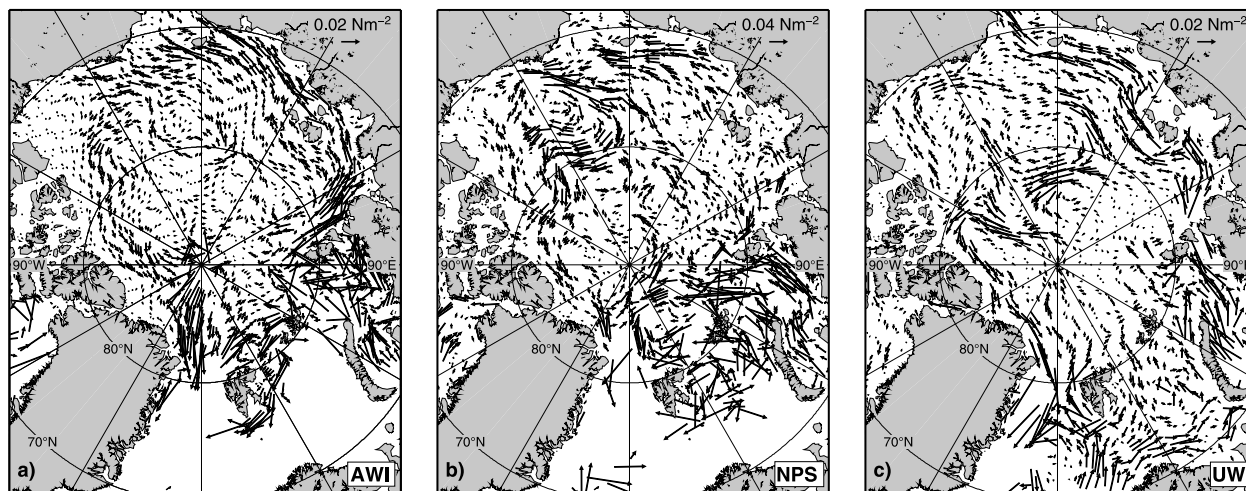


Figure 9. Ocean-sea ice stress difference $\tau_{\text{ioc}} - \tau_{\text{oc}}$ (see details in the main text) for (a) AWI, (b) NPS, and (c) UW models averaged over winter 1994/1995 corresponding to sea ice drift means in Figure 8. For clarity reasons the horizontal resolution is individually reduced and only stresses smaller than 0.05 N m^{-2} (NPS: 0.1 N m^{-2}) are shown. Note different scaling in Figure 9b.

forcing are only partly responsible for the different sea ice drift statistics as the AWI 10-m-wind run tends toward higher drift speeds but is still closer to the results of the first than those of the second group of models.

[23] The coupled sea ice-ocean models differ in the detail of the dynamic coupling to the ocean. Some apply the technique of *Hibler and Bryan [1987]* where the uppermost grid cell of the ocean is thought of as a mixture of sea ice and water and where the momentum forcing of the mixture contains the wind stress and the internal sea ice stresses. Other ocean models are driven with the sea ice-ocean drag when ice covered. These differences have only an indirect effect on the sea ice drift through changes in ocean circulation. Models further differ in the ocean velocity that enters the ocean drag in the sea ice model. It is the choice of the modeling group to use first ocean level velocities, directly or subject to a turning angle, or some approximation to the geostrophic velocity. The latter is usually the velocity of the second ocean model level, which is already below the Ekman layer, combined with an assumption about the veering of the currents that are relevant for the sea ice drift. For instance, the AWI model employs the ocean velocity of the second layer centered at 15 m depth with a turning angle of 25° . NPS and UW models use the one of the second and fourth layer respectively, both centered at 35 m, without a turning angle. For reasons of the stability of the sea ice model, at least the AWI model employs an average over a few days of the oceanic currents that enter the drag term. We found that the applied ocean velocities do not vary in speed to an extent that explains the large ice drift speed of the NPS model. The absolute values of ocean speeds are similar between AWI and NPS models. That means that the ocean-ice stress of the NPS model is dominated by the large ice drift speed. Correspondingly, the NPS ice-ocean stress is approximately twice as large as in the AWI and UW models. To illustrate the oceanic influence on the sea ice momentum balance we compiled not only the real ocean stress, effected by ocean and ice velocity τ_{oc} , but also an ocean stress τ_{ioc} with an inactive

ocean ($u_{\text{oc}} = 0.0 \text{ m s}^{-1}$). The difference $\tau_{\text{ioc}} - \tau_{\text{oc}}$ presented in Figure 9 for the winter 1994/1995 for AWI, NPS and UW models then shows the pure influence of the ocean velocity on the ocean-ice stress. There are three points of particular interest for this winter mean. The first finding is the opposite direction of $\tau_{\text{ioc}} - \tau_{\text{oc}}$ comparing AWI result to NPS and UW along the Alaskan coast. The oceanic part of the ocean-ice stress in the AWI model is found to be directed opposite to the AOMIP wind stress direction and thus hinders the ice to drift westward along the coastline. This leads to the weak ice drift found in the AWI model in this region (Figure 8a). In the NPS and UW models the ocean velocity is clearly dominant compared to the low ice velocity and drives the ice westward along the coastline to follow the remnants of the Beaufort Gyre (Figure 8c), supporting the wind stress in this case. The second observation is that an eastward sea ice drift in the East Siberian Sea is strongly supported by the oceanic momentum flux in AWI, NPS, and UW models. A strong eastward ocean movement in the East Siberian Sea results in ice drift in the same direction because of the again weak AOMIP wind-forcing in this region. Other wind stress forcings, 10-m-wind derived and NCEP/NCAR momentum flux, would support this eastward ice drift, which is present in the observational data only to a minor degree (compare Figure 1). A third finding explains the difference in ice drift between AWI, NPS and UW models concerning the strong cyclonic gyre in winter 1994/1995. Only the UW result does not show a closed gyre in the region around 80°N and 180°E . Here the strong impact of the ocean velocity and its matching direction are again the reason why the UW model features the largest deviation to the wind-forcing, which improves the drift pattern in this case. Figure 9c shows that the ocean hinders the ice to follow the cyclonic pattern west of 180°E and north of 80°N . While the NPS model does not feature a coordinated current in this particular region that would hinder the cyclonic ice drift, this drift is even supported by the ocean velocity in the AWI result (Figures 9a and 9b). However, it should not be

Table 3. Sea Ice Volume Transport Through Fram Strait Averaged Over the Period August 1990 to July 1996 and Compared to Monthly Means of Observational Data From *Vinje et al.* [1998]

Data Set	Mean Volume Export, km ³ month ⁻¹	Standard Deviation km ³ month ⁻¹	Correlation Coefficient to Data From <i>Vinje</i> <i>et al.</i> [1998]
AWI	239	157	0.72
GSFC	110	64	0.72
IOS	339	221	0.62
NPS	322	228	0.66
UW	113	105	0.67
<i>Vinje et al.</i> [1998]	237	142	(1.0)

forgotten that the wind-forcing causes the dominant cyclonic gyre in sea ice drift. This gyre is not found in the observational data. It is a strong feature in the NCEP/NCAR reanalysis data that is already present in the SLP field (Figure 8d).

[24] The main findings concerning the comparison of the impact of wind and ocean stress on the ice drift is also supported by the second example we focused on, the cyclonic and anticyclonic drift regimes: The sea ice drift of the AWI model follows closely the provided wind-forcing, which has also the strongest impact on the upper ocean velocity field compared to NPS and UW model. A reason for this difference between models may be the different depth where the ocean velocities applied for the ocean-ice stress are centered (AWI 15 m and NPS, UW 35 m). For the NPS model holds that the ice drift dominates the ocean-ice stress. Thus the cause for the large ice drift speeds of the NPS model are most probably found in the sea ice model implementation. Our investigations of the UW results on the other hand show that the ocean velocity is the dominant part of the ocean-ice stress in certain regions, namely along the coast lines of East Siberian, Beaufort and Lincoln seas as well as in parts of the cyclonic gyre in the central Arctic described above. Here the UW model ocean stress outbalances the comparatively weak wind-forcing.

[25] Differences in ocean-ice stress can have a number of reasons. We have already mentioned the strategies followed by different groups in coupling ocean and sea ice components. The different stresses that enter the ocean component could also play an important role in the differences in the oceanic velocity itself. Because of the small planetary- β at high latitudes, the Sverdrup relationship implies large changes in the horizontal velocity components in response to changes in Ekman pumping velocity. In those models following the approach of *Hibler and Bryan* [1987] the Ekman pumping velocity is determined by the wind stress while in other models the ocean-ice drag determines the Ekman pumping.

[26] Apart from the differences between the single models, it is disconcerting to note the rather large and systematic differences between the models and observations for the extreme winter of 1994/1995. The differences imply that incorrect regions of the Arctic Ocean could feed the Fram Strait ice export in the models. This could lead to wrong interpretations of palaeodata (sediment transport with the ice) and false predictions for Fram Strait ice export that are based on the upstream conditions and developments in the interior Arctic. Apart from these upstream differences we found that ice area and volume exports through Fram Strait

are represented well by the AWI model of the first group of models and overestimated by the second group of models (IOS, NPS) owing to their large drift speeds (see Table 3). However, GSFC and UW models tend to underestimate ice volume and thus feature a smaller ice export under AOMIP forcing. This underestimate could be related to the overall thinner ice in those models. The extreme ice export event in the winter 1994/1995 is, however, determined by a positive drift speed anomaly in Fram Strait and not by anomalously thick ice in all models. The ice export in the winter 1994/1995 appears to be given by the local winds in Fram Strait such that the mismatch between observed and simulated drift pattern in the interior Arctic does not affect the southward volume transport anomaly.

[27] Despite the regionally important influence of the oceanic circulation on sea ice drift, the large-scale sea ice drift in the winter 1994/1995 is governed by the prescribed wind stress. Differently generated wind stress fields (SLP derived, 10-m-wind derived or the wind stress taken directly from reanalysis) all include a strong cyclonic forcing over the central Arctic Ocean that is reflected in a pronounced cyclonic sea ice drift. Furthermore, both AWI model experiments, the AOMIP-forced and the 10-m-wind forced versions show similar biases in drift speed and direction in the East Siberian Sea and north of it in the central Arctic. These biases are also observed for the other AOMIP models. Actually, the AWI 10-m-wind experiment features slightly larger drift speeds (Figure 3) and thus the absolute values of AOMIP wind stress seem to be more realistic than those of wind stress alternatives. This holds not for the direction as stated before. We conclude that the reanalysis data used to derive the atmospheric forcing include uncertainties. These errors can never be excluded completely, because direct measurements are sparse in this region.

[28] The mean vorticities calculated from the NSIDC sea ice drift observations do not reflect the CCR and ACCR. Neither do the model results. The correlations between observed and simulated sea ice drift vorticity is between 0.5 and 0.7 (see Table 2). A likely reason for the relatively weak correlation is the basic difference between modeled and observed drift patterns as described above. The chosen positions for calculating the vorticity of the Beaufort Gyre does not necessarily match the observed drift conditions though it is well suited to compare the model results.

[29] For all models it holds that the summer mean (May to October) is in nearly all cases less anticyclonic/more cyclonic than the adjoining winter means (November to April). This agrees with the description of *Proshutinsky et al.* [2002]. However, the time series (Figure 7) and mean

values (Table 2) of vorticity of all models agree only partly with the circulation regime phases of *Proshutinsky et al.* [2002]. The number of cyclonic events or their intensity does not change explicitly between the regimes, though the long cyclonic phase of 1989–1997 exhibits more events than before or after this period, at least in the AWI and GSFC data and within the years spanned by our investigation. The most prominent cyclonic event in 1994/1995 coincides with the observed maximum in sea ice export through Fram Strait. A possible reason for the mismatch between ice drift and regime phases in Figure 7 is the derivation of the regimes by *Proshutinsky and Johnson* [1997]. They distinguished the regime phases from the interannual variability of the sea surface height gradient. The latter was derived using a two-dimensional, wind-driven, barotropic ocean model coupled with a dynamic sea ice model. This model and its forcing deviate considerably from those examined here and it is conceivable that surface heights in the AOMIP models will be different. The sea surface height determines the sea surface pressure gradient force that enters the momentum balance of sea ice drift. As stated above this force plays a negligible role except for the Beaufort Gyre. Exactly the strength of this feature is important for the difference between the two drift regimes. However, the surface wind transition coefficients and turning angles are the same as used in the AOMIP models that are described in section 3.

6. Conclusions

[30] Numerical sea ice-ocean models are potentially very powerful tools to study physical processes in the Arctic Ocean and to explain principal relationships between forcing fields and oceanic and sea ice variables. For the first time, five different sea ice-ocean coupled models for the entire Arctic are compared regarding sea ice drift. Furthermore, two independent observational data sets of comparable horizontal resolution and data density are taken into account. Despite very similar experimental settings and coupled sea ice-ocean models that represent the state-of-the-art, we find two categories of sea ice drift speeds among the results: one with a well pronounced, lower modal speed, matching the observations best, and a second with a more even speed distribution featuring also higher drift speeds. We also compared the drift patterns of the models in two case studies: the difference between two wind-driven circulation regimes and the extraordinary winter of 1994/1995. For the first case all models show equal patterns of drift difference between regimes. The sensitivity of the models to anomalous forcing differs. The response in the direction of the drift is very similar, on the other hand. For the second case models revealed differences in winter mean drift pattern. These differences cannot be assigned to the different speed classes and have different reasons. Taking individual model parameters into account, no clear consistency or explanation for the differences between the model results is found. Still, owing to the model physics, the most plausible reason lies in the different effective wind stress forcing and in the coupling with the ocean. Besides the coupling mechanism itself, which controls the intensity of the effect that the ocean has on the ice, the different ocean velocities of the models are found to cause some of the

observed differences in ice drift pattern. A strong ocean influence on the ice drift coincides most often, though not always, with a weak wind stress forcing. Furthermore, the numerical implementation of the model physics often differs and the resulting sea ice drift, concentration and thickness are definitely sensitive to the implementation. At this stage of the investigation on sea ice drift estimates from models and observations no clear recommendation concerning the choice of parameters can be offered to the modeling community. Nevertheless, we found that the calculation of the transfer of momentum from the atmosphere to the ice is critical to the sea ice drift. The sensitivity to ocean drag and coupling methods needs to be studied closely as a next step. As implementation methods were out of scope here sensitivity studies concerning atmospheric and ocean drag as well as sea ice parameters should be done with one and the same model in order to get a direct handle on the various causes for differences in sea ice motion.

[31] **Acknowledgments.** We acknowledge the support of the European Union through the INTAS project “Nordic Seas” and the ESA through the GLOBICE project. We thank the involved AOMIP groups for supplying the data and Mark Johnson and Steve Gaffigan for early results from their model comparison. We also thank our Associate Editor and reviewers for inspiring comments. Satellite data were provided by NSIDC, Boulder, Colorado (USA) and by CERSAT at IFREMER, Plouzané (France). The buoy data were provided by the International Arctic Buoy Program, PSC, APL, University of Washington, Seattle, Washington (USA). This research is supported by the National Science Foundation Office of Polar Programs under Cooperative Agreements OPP-0002239 and OPP-0327664 with the International Arctic Research Center, University of Alaska Fairbanks.

References

- Emery, W. J., C. W. Fowler, and J. A. Maslanik (1997), Satellite-derived maps of Arctic and Antarctic sea ice motion: 1988 to 1994, *Geophys. Res. Lett.*, *24*(8), 897–900.
- Ezraty, R., and J. F. Piollé (2004), Sea-ice drift in the central Arctic combining QuikSCAT and SSM/I sea ice drift data—User’s manual (v1.0, April 2004), report, Cent. ERS d’Arch. et de Traitement, IFREMER, Brest, France.
- Fowler, C. (2003), Polar Pathfinder daily 25 km EASE-grid sea ice motion vectors, <http://nsidc.org/data/nsidc-0116.html>, Natl. Snow and Ice Data Cent., Boulder, Colo.
- Harder, M., P. Lemke, and M. Hilmer (1998), Simulation of sea ice transport through Fram Strait: Natural variability and sensitivity to forcing, *J. Geophys. Res.*, *103*(C3), 5595–5606.
- Hibler, W. D. (1979), A dynamic thermodynamic sea ice model, *J. Phys. Oceanogr.*, *9*, 815–846.
- Hibler, W. D., III, and K. Bryan (1987), A diagnostic ice-ocean model, *J. Phys. Oceanogr.*, *17*, 987–1015.
- Holloway, G., et al. (2007), Water properties and circulation in Arctic Ocean models, *J. Geophys. Res.*, doi:10.1029/2006JC003642, in press.
- Hunke, E. C., and J. K. Dukowicz (1997), An elastic-viscous-plastic model for sea ice dynamics, *J. Phys. Oceanogr.*, *27*, 1849–1867.
- Johnson, M., S. Gaffigan, E. Hunke, and R. Gerdes (2007), A comparison of Arctic Ocean sea ice concentration among the coordinated AOMIP model experiments, *J. Geophys. Res.*, doi:10.1029/2006JC003690, in press.
- Kalnay, E., et al. (1996), The NCEP/NCAR 40-Year Reanalysis Project, *Bull. Am. Meteorol. Soc.*, *77*, 437–495.
- Kreyscher, M., M. Harder, P. Lemke, and G. M. Flato (2000), Results of the Sea Ice Model Intercomparison Project: Evolution of sea ice rheology schemes for use in climate simulations, *J. Geophys. Res.*, *105*(C5), 11,299–11,320.
- Kwok, R., A. Schweiger, D. A. Rothrock, S. Pang, and C. Kottmeier (1998), Sea ice motion from satellite passive microwave imagery assessed with ERS SAR and buoy motions, *J. Geophys. Res.*, *103*(C4), 8191–8214.
- Lemke, P., W. D. Hibler, G. Flato, M. Harder, and M. Kreyscher (1997), On the improvement of sea ice models for climate simulations: The Sea Ice Model Intercomparison Project, *Ann. Glaciol.*, *25*, 183–187.
- Martin, T., and T. Martin (2006), Anomalies of sea ice transports in the Arctic, *Ann. Glaciol.*, *44*, in press.

- Maslanik, J., T. Agnew, M. Drinkwater, W. Emery, C. Fowler, R. Kwok, and A. Liu (1998), Summary of ice-motion mapping using passive microwave data, *Spec. Publ. 8*, Natl. Snow and Ice Data Cent., Boulder, Colo.
- Mellor, G. L., and L. H. Kantha (1989), An ice-ocean coupled model, *J. Geophys. Res.*, *94*(C8), 10,937–10,954.
- Ortmeyer, M., and I. G. Rigor (2004), International Arctic Buoy Program data report 2003, *Tech. Memo. APL-UW TM 2-04*, Appl. Phys. Lab., Univ. of Wash., Seattle.
- Proshutinsky, A., and M. A. Johnson (1997), Two circulation regimes of the wind driven Arctic Ocean, *J. Geophys. Res.*, *102*(C6), 12,493–12,514.
- Proshutinsky, A., R. H. Bourke, and F. A. McLaughlin (2002), The role of the Beaufort Gyre in Arctic climate variability: Seasonal to decadal climate scales, *Geophys. Res. Lett.*, *29*(23), 2100, doi:10.1029/2002GL015847.
- Rigor, I. G., J. M. Wallace, and R. L. Colony (2002), Response of sea ice to the Arctic Oscillation, *J. Clim.*, *15*(18), 2648–2663.
- Thomas, D. (1999), The quality of sea ice velocity estimates, *J. Geophys. Res.*, *104*(C6), 13,627–13,652.
- Vinje, T., N. Nordlund, and A. Kvambekk (1998), Monitoring ice thickness in Fram Strait, *J. Geophys. Res.*, *103*(C5), 10,437–10,450.
-
- R. Gerdes and T. Martin, Alfred Wegener Institute for Polar and Marine Research, P. O. Box 120161, D-27515 Bremerhaven, Germany. (torge.martin@awi.de)